LAWRENCE
LIVERMORE
NATIONAL
LABORATORY

LLNL-JRNL-648769

Ballooning modes localized near the null point of a divertor

W. A. Farmer

January 29, 2014

Physics of Plasmas

Disclaimer

This document was prepared as an account of work sponsored by an agency of the United States government. Neither the United States government nor Lawrence Livermore National Security, LLC, nor any of their employees makes any warranty, expressed or implied, or assumes any legal liability or responsibility for the accuracy, completeness, or usefulness of any information, apparatus, product, or process disclosed, or represents that its use would not infringe privately owned rights. Reference herein to any specific commercial product, process, or service by trade name, trademark, manufacturer, or otherwise does not necessarily constitute or imply its endorsement, recommendation, or favoring by the United States government or Lawrence Livermore National Security, LLC. The views and opinions of authors expressed herein do not necessarily state or reflect those of the United States government or Lawrence Livermore National Security, LLC, and shall not be used for advertising or product endorsement purposes.

Ballooning modes localized near the null point of a divertor

W. A. Farmer[1, 2]

[1)] *Physics and Astronomy Department, University of California Los Angeles, Los Angeles, California 90095, USA*

[2)] *Lawrence Livermore National Laboratory, 7000 East Ave., Livermore, CA 94550, USA*

(Dated: 27 January 2014)

The stability of ballooning modes localized to the null point in both the standard and snowflake divertors is considered. Ideal magnetohydrodynamics is used. A series expansion of the flux function is performed in the vicinity of the null point with the lowest, non-vanishing term retained for each divertor configuration. The energy principle is used with a trial function to determine a sufficient instability threshold. It is shown that this threshold depends on the orientation of the flux surfaces with respect to the major radius with a critical angle appearing due to the convergence of the field lines away from the null point. When the angle the major radius forms with respect to the flux surfaces exceeds this critical angle, the system is stabilized. Further, the scaling of the instability threshold with the aspect ratio and the ratio of the scrape-off-layer width to the major radius is shown. It is concluded that ballooning modes are not a likely candidate for driving convection in the vicinity of the null for parameters relevant to existing machines. New importance is given to an axisymmetric mixing mode [Farmer and Ryutov, Phys. Plasmas **20**, 092117 (2013)] as a likely candidate to explain current experimental results.

I. INTRODUCTION

The heat loads on the divertor plates in a fusion reactor are expected to be well beyond the limits of currently existing materials. For this reason, much effort is being exerted to find novel ways to reduce heat loads on the divertor plates. One such idea is the snowflake divertor, named for the characteristic hexagonal structure of the separatrices. This hexagonal structure is due to the presence of a second order null in the poloidal field, i.e. $B_p \propto d^2$ where B_p is the magnitude of the poloidal field and d is the distance from the null point in the poloidal plane[1,2]. For comparison, a standard divertor configuration has $B_p \propto d$, and the separatrices form a characteristic 'X' shape. Because of this quadratic dependence on the field strength, the snowflake divertor is believed to have many different positive effects leading to a reduction of heat loads on the divertor plates[3]. One reason for this is that the region over which $\beta_p = 8\pi p/B_p^2 \gg 1$, where p is the plasma pressure, is much larger in the snowflake than in the standard divertor[4,5]. The effects of large β_p combined with unfavorable curvature of the magnetic field can drive plasma instability, resulting in plasma convection in the divertor region[4,5]. The resulting convection can lead to heat transport across the separatrices, and because of the hexagonal structure in the snowflake, the resulting heat flux would be deposited upon four strike points instead of the two that exist in the standard divertor. Recently, the consequences of a third-order null leading to a "cloverleaf" divertor have also been considered[6]. Such a divertor would lead to even more intense convection, though the feasibility of producing such a divertor in the laboratory is not yet clear.

The snowflake divertor has been realized experimentally on the tokamaks, NSTX[7,8], TCV[9–11], and DIII-D[12] and it has been shown to lead to a reduction in heat flux. Further, on TCV it has been observed that the heat flux was split over multiple strike points[13,14], suggesting that convection is indeed occurring in the divertor region. It is important to determine the precise mechanism which is driving this convective process in order to optimize the reduction in heat loads. The first possibility is that the plasma equilibrium, commonly assumed to be well approximated by the vacuum fields, is lost due to the presence of a toroidal current in the vicinity of the null point[15]. This absence of equilibrium would allow for transport of plasma into the private flux region. If plasma equilibrium is maintained, instability could also lead to enhanced transport. Two types of instabilities are most likely. The first candidate, which has been considered in a model geometry, is that of an axisymmet-

ric, curvature-driven instability[16]. Because the instability is axisymmetric, it corresponds to an $n = 0$ mode and is not coupled to toroidal motion of the plasma. Further, an axisymmetric perturbation leaves the toroidal field unperturbed. This is energetically favorable due to the strength of the toroidal field. The second candidate iso that of a ballooning mode which varies rapidly transverse to the magnetic field, but slowly in the direction of the field lines. In this case, the energy of perturbing the magnetic field is offset by the slow variation of the perturbation along the field line. It is this instability which we wish to consider here.

The theory of ballooning modes was first fully developed for the ideal MHD equations for closed magnetic field lines by Connor, Hastie, and Taylor[17]. Since then, many papers have been published about ballooning modes, and the theory is found in various reviews and textbooks, e.g.[18]. In considering ballooning modes in the divertor region, the biggest difference is that the field lines are now open and intersect the conducting end plates. This changes the boundary condition from the periodic boundary condition present in the core plasma. A great simplification is to treat the boundary plates as perfect conductors and require line-tying boundary conditions at the plates. In reality, the formation of a plasma sheath results in incomplete line-tying and lowers the growth rates of interchange modes[19]. To properly account for these sheath boundary conditions, one must move beyond an ideal MHD description to a two-fluid model for the plasma. These modes have been investigated in detail using a Braginskii fluid model for the standard divertor to ascertain plasma stability[20] and linear and non-linear evolution of ballooning modes[21] in the scrape-off-layer (SOL). In the context of ideal MHD, the effects of insulating, resistive, and conducting boundary conditions on ballooning modes occurring along open field lines have been investigated[22]. While these effects are certainly relevant, we desire to ascertain the effects of the complex geometry present in the vicinity of the null point. To this end, we apply ideal MHD to the plasma existing in the vicinity of the null point. Because the modes considered are localized to this region, the resulting instability condition will be less strict than theories which describe the core plasma and include the x-point in the analysis, for example, Webster and Gimblett's analysis of peeling modes near the separatrix[23]. The modes considered here will have different consequences, being responsible for dynamics isolated to the null point. This should be sufficient for ascertaining whether ballooning modes could be responsible for the enhanced convection observed on TCV[13,14], while giving general analytic relations that can be applied to any device.

The outline of the paper is as follows. In section II, the geometry of the flux surfaces for both the standard and snowflake divertors is presented. In section III, the ballooning mode formalism is summarized and applied to both the standard and snowflake divertors. In section IV, a test function is used in the energy principle to derive an instability threshold. Conclusions are presented in section V. Finally, a simpler model geometry used in Ref. 16 is considered in the Appendix in order to compare to the axisymmetric instability.

II. GEOMETRY OF STANDARD AND SNOWFLAKE DIVERTORS

In describing the divertor geometry, we do so in the vicinity of the null point of the poloidal field. All equilibrium quantities are assumed to be independent of the toroidal coordinate, ζ. In describing the poloidal plane, two coordinate systems are used, and relations between the two will be given later in this section. The first is a Cartesian coordinate system, (x, z), defined such that the origin is located at the null point. Since we are performing the analysis in the vicinity of the null, the ordering of spatial scales is $|x|, |z| \ll a < R$, where a and R are the minor and major radii, respectively. With these assumptions, $\nabla\zeta = \hat{\boldsymbol{\zeta}}/R$. Flux coordinates are also used because they allow for a simple form for the equations governing the ballooning mode. Thus, the flux surface and generalized poloidal angle are denoted by ψ and χ, respectively. Because of the spatial orderings, the straight, cylindrical approximation will be made in both coordinate systems, but the use of flux coordinates allows for the accurate description of the complicated magnetic geometry in the vicinity of the null point. In flux coordinates, the poloidal field can be written as

$$\mathbf{B}_p = \nabla\psi \times \nabla\zeta. \tag{1}$$

The standard assumption that there is no toroidal current near the null point leads to the equation,

$$\nabla \times \mathbf{B}_p = -\nabla\zeta\nabla^2\psi = 0. \tag{2}$$

The Laplacian which acts on ψ can be simplified if the torus is treated in the straight-cylindrical approximation. In this case, the equation reduces to

$$\left(\frac{\partial^2}{\partial x^2} + \frac{\partial^2}{\partial z^2}\right)\psi = \left[\frac{1}{r}\frac{\partial}{\partial r}\left(r\frac{\partial}{\partial r}\right) + \frac{1}{r^2}\frac{\partial^2}{\partial\theta^2}\right]\psi = 0, \tag{3}$$

where $r = \sqrt{x^2 + z^2}$ and $\theta = \tan^{-1}(x/z)$ are the familiar polar coordinates. From here, it is clear that the solutions can be expanded in terms of sinusoidal harmonics each with their

own radial dependence. Additionally, since the fields must be bounded at the origin, the flux function can be written as

$$\psi = \sum_{m=0}^{\infty} \left(\frac{r}{a}\right)^m \left(A_m \cos(m\theta) + B_m \sin(m\theta)\right), \tag{4}$$

with A_m and B_m being constants that determine the specific expansion of the flux function about the origin. The constant term, $m = 0$, does not effect the poloidal field as $\mathbf{B}_p$ is related to ψ through a derivative. The $m = 1$ term corresponds to a non-vanishing field at the origin. Such a field is relevant to the model geometry in Ref. 16, and is considered in the Appendix. Here, the $m = 1$ term is discarded. The $m = 2$ term is the dominant term for the standard divertor in the vicinity of the null, the $m = 3$ term for the snowflake, and the $m = 4$ term for the cloverleaf. For this reason, we approximate the flux function for the standard divertor in the vicinity of the null point as

$$\psi = C\frac{B_{pM}Ra}{2}\left(\frac{r}{a}\right)^2 \cos(2\theta) = CB_{pM}Ra\left(\frac{x^2 - z^2}{2a^2}\right), \tag{5}$$

and for the snowflake divertor,

$$\psi = C\frac{B_{pM}Ra}{3}\left(\frac{r}{a}\right)^3 \cos(3\theta) = CB_{pM}Ra\left(\frac{x^3 - 3xz^2}{3a^3}\right). \tag{6}$$

In the above expressions, the constant has been determined by considering the asymptotic value of the flux function as $r \sim a$. In this limit, $B_p = |\nabla\psi|/R \sim B_{pM}$, the strength of the poloidal field in the midplane. The specific choice of a cosine represents a specific orientation of the flux surfaces. To retain generality in this formulation, the major radius is assumed to form an angle, α, with the x-axis. It is true that higher order terms in the expansion may contribute at distances from the origin that are on the order of the minor radius, but we approximate the surfaces to lowest, non-vanishing order, consistent with the length scales in the problem. Additionally, the lowest order terms given are proportional to a constant of order unity, C, which depends on the specific global geometry of the problem. These constants of order unity can be determined by considering the global geometry for a specific device.

In determining the generalized poloidal coordinate for this geometry, a degree of freedom exists. For convenience, we choose $|\nabla\chi| = |\nabla\psi|$. This choice causes χ to be harmonically conjugate to ψ. The form of χ is easily found for the standard divertor to be

$$\chi = C\frac{B_{pM}Ra}{2}\left(\frac{r}{a}\right)^2 \sin(2\theta) = CB_{pM}Ra\left(\frac{xz}{a^2}\right), \tag{7}$$

and for the snowflake divertor to be

$$\chi = C\frac{B_{pM}Ra}{3}\left(\frac{r}{a}\right)^3 \sin(3\theta) = CB_{pM}Ra\left(\frac{3x^2z - z^3}{3a^3}\right). \tag{8}$$

Further, a complex flux function can be defined in this case to be

$$\eta = \psi + i\chi = C\frac{B_{pM}Ra}{m}\left(\frac{r}{a}\right)^m \exp(im\theta) = C\frac{B_{pM}Ra}{m}\left(\frac{x+iz}{a}\right)^m, \tag{9}$$

where $m = 2$ corresponds to the standard divertor and $m = 3$ to the snowflake. The form of the above function is convenient in that it is easily inverted so that the coordinates, (x, z), can be expressed analytically in terms of their counterparts, (ψ, χ). This would not be the case if higher order terms were present in the expansions or if a toroidal current were present in the vicinity of the null, causing ψ to no longer be a harmonic function.

Next, the jacobian of the flux coordinate system can be determined from the relation

$$\frac{1}{J} = \nabla\chi \cdot (\nabla\psi \times \nabla\zeta). \tag{10}$$

This can be done for arbitrary m using Eq. (9) to compute the necessary gradients. If this is done, the following equation results,

$$\frac{1}{J} = C^2RB_{pM}^2\left(\frac{x^2+z^2}{a^2}\right)^{m-1} = C^2RB_{pM}^2\left(\frac{m^2(\psi^2+\chi^2)}{C^2B_{pM}^2R^2a^2}\right)^{\frac{m-1}{m}}. \tag{11}$$

Setting $m = 2$ gives the following result for the standard divertor,

$$\frac{1}{J} = C^2RB_{pM}^2\left(\frac{x^2+z^2}{a^2}\right) = 2C^2RB_{pM}^2\left(\frac{\psi^2+\chi^2}{C^2R^2a^2B_{pM}^2}\right)^{1/2}, \tag{12}$$

and $m = 3$ for the snowflake divertor gives,

$$\frac{1}{J} = C^2RB_{pM}^2\left(\frac{x^2+z^2}{a^2}\right)^2 = 3^{4/3}C^2RB_{pM}^2\left(\frac{\psi^2+\chi^2}{C^2R^2a^2B_{pM}^2}\right)^{2/3}. \tag{13}$$

Additionally, because of the choice that $|\nabla\chi| = |\nabla\psi|$, a useful relation between the jacobian, the magnitude of the poloidal field, and the major radius is

$$B_p^2RJ = 1. \tag{14}$$

This relation will be used later to simplify various expressions.

Figure 1 shows the flux surface geometry both in the standard and snowflake divertors. The surfaces of constant ψ are shown as black curves, and the surfaces of constant χ as

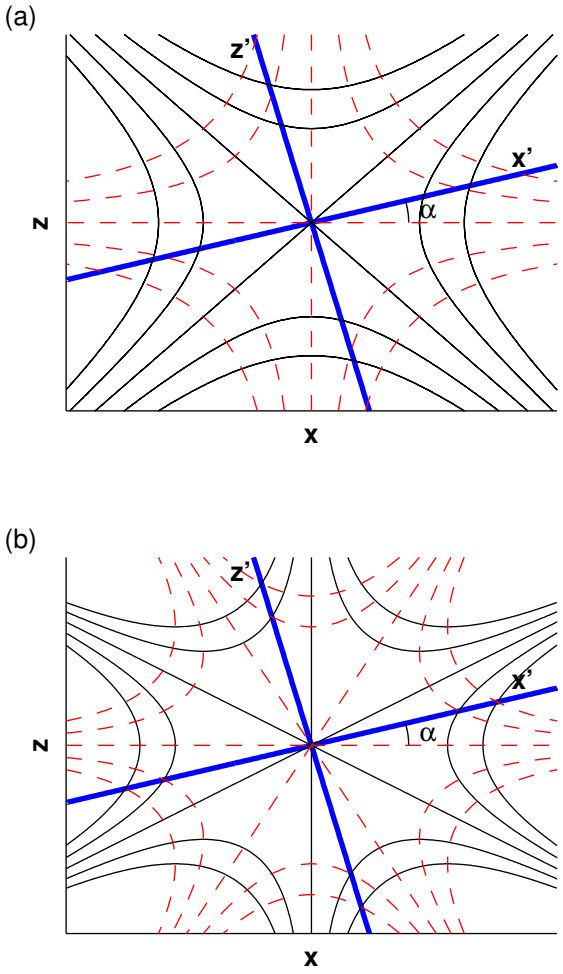

FIG. 1. Geometry of flux surfaces in the vicinity of the poloidal null. (a) Standard divertor, (b) snowflake divertor. Solid black lines are surfaces of constant ψ and dashed red lines are surfaces of constant χ. The thick blue lines indicate an alternate choice of (x, z) axes in which the flux surfaces are rotated through an angle, α. Here, it is assumed that the machine center and the toroidal curvature lies in the $-x'$ direction. The toroidal direction lies out of the board.

dashed red curves. The separatrices are represented by the straight black lines. The upper panel shows the characteristic 'X' shape of the separatrix present in the standard divertor, and the poloidal plane is divided into four disjoint regions in which the magnetic field lines are separated from the other regions. The lower panel shows the characteristic hexagonal shape of a pure snowflake divertor. In both panels, a second set of axes, (x', z'), is illustrated

by the thick blue lines. This reflects the arbitrary direction of the major radius which is taken to form the angle, α, with the x-axis.

III. BALLOONING MODE EQUATIONS

The ballooning mode formalism has been discussed in many places, e.g.[17,18,20–22], and we refer the reader to these references for a more detailed presentation. For simplicity, we assume that perfectly conducting plates are present in the poloidal plane, and that these surfaces are defined at a constant χ. Defining the plasma displacement to be $\boldsymbol{\xi}$, then the boundary conditions are simply that each component of $\boldsymbol{\xi}$ must vanish at the plates. Because of these boundary conditions, the component of $\boldsymbol{\xi}$ parallel to the magnetic field which Hameiri retains[22] decouples from the perpendicular motion when minimizing the energy to find the most unstable mode. This allows the differential equations to be reduced to an uncoupled equation for the perpendicular plasma displacement in which the parallel displacement is chosen to minimize the energy.

Adopting the presentation used by Freidberg[18], an eikonal approximation is first made for the plasma displacement which takes the form

$$\boldsymbol{\xi} = \boldsymbol{\eta} e^{in\left(\zeta - \int_{\chi_0}^{\chi} \nu \, d\chi'\right)}, \tag{15}$$

where n corresponds to the toroidal mode number. The quantity, ν is chosen so that the phase in the exponential is constant along a field line and is expressed as $\nu = B_t J/R$, where B_t is the toroidal field strength. From this eikonal approximation, the perpendicular wave vector can be found by taking the gradient of the eikonal. This results in

$$\mathbf{k}_\perp = -n \left(\int_{\chi_0}^{\chi} \frac{\partial \nu}{\partial \psi} \, d\chi' \right) \nabla\psi + n \left(\nabla\zeta - \nu \nabla\chi \right), \tag{16}$$

$$= k_n \hat{\boldsymbol{\psi}} + k_t \hat{\mathbf{t}}, \tag{17}$$

where the wave vector has been resolved into two components: k_n, the portion normal to the flux surfaces; and k_t, lying orthogonal to both the normal to the flux surfaces and the magnetic field, parallel to the vector $\hat{\mathbf{t}} = \hat{\boldsymbol{\zeta}} B_p/B - \hat{\boldsymbol{\chi}} B_t/B$. From Eqs. (1) it can be shown

that $|\nabla\psi| = B_p R$. Further, since we have chosen $|\nabla\psi| = |\nabla\chi|$, k_n and k_t can be written as

$$k_n = -nRB_p \int_{\chi_0}^{\chi} \frac{\partial \nu}{\partial \psi}\, d\chi', \tag{18}$$

$$k_t = n\frac{B}{RB_p}. \tag{19}$$

Next, to minimize the energy, $\boldsymbol{\eta}_\perp$ is to lowest order,

$$\boldsymbol{\eta}_\perp = \frac{X}{nB}\hat{\mathbf{b}} \times \mathbf{k}_\perp. \tag{20}$$

Here, B is the total magnetic field strength, and $\hat{\mathbf{b}}$ is a unit vector in the direction of the magnetic field. The n in the denominator is introduced here to keep the perturbed energies and fields of order unity. With these definitions, the energy principle for the ballooning mode is given by

$$\omega^2 = \frac{W}{K}, \tag{21}$$

$$W = \frac{1}{4}\int d\psi\, W(\psi), \tag{22}$$

$$W(\psi) = \frac{1}{n^2}\int J d\chi \left[\frac{1}{J^2B^2}\left(k_n^2 + k_t^2\right)\left|\frac{\partial X}{\partial \chi}\right|^2 - \frac{8\pi RB_p}{B^2}\frac{dp}{d\psi}\left(k_t^2\kappa_n - k_t k_n \kappa_t\right)|X|^2\right], \tag{23}$$

$$K = \frac{\pi}{n^2}\int J d\psi d\chi\, \frac{\rho(k_n^2 + k_t^2)}{B^2}|X|^2, \tag{24}$$

where the plasma displacement is assumed to have harmonic time dependence, $\exp(-i\omega t)$. If $\omega^2 < 0$, this corresponds to instability and exponential growth of the perturbation. The quantity, $-\omega^2 K$, corresponds to the perpendicular kinetic energy with the parallel kinetic energy neglected. This is done as in the original paper by Connor, et al.[17] in order to simplify the resulting equations. This simplification does not alter the resulting instability thresholds derived, though it may overestimate predicted growth rates. The potential energy change caused by the perturbation is given by W. As expressed in the equations, the integrand only depends on ψ as a parameter, and as a result, the analysis can be performed on each flux surface independently of the other flux surfaces, reflecting the one-dimensional property that occurs when the ballooning limit is taken. The quantities, ρ and p represent the plasma mass density and pressure, respectively, and $\boldsymbol{\kappa}$ corresponds to the curvature of the magnetic field. The magnetic curvature is resolved into two components, $\boldsymbol{\kappa} = \kappa_n\hat{\boldsymbol{\psi}} + \kappa_t\hat{\mathbf{t}}$, just as $\mathbf{k}_\perp$ is. The magnetic curvature is defined to be $\boldsymbol{\kappa} = \hat{\mathbf{b}}\cdot\nabla\hat{\mathbf{b}}$. From this definition and the plasma

equilibrium, it can be shown that

$$\boldsymbol{\kappa} = -\frac{4\pi}{B^2}\hat{\mathbf{b}} \times \left[\hat{\mathbf{b}} \times \nabla\left(p + \frac{B^2}{8\pi}\right)\right], \tag{25}$$

$$= \frac{4\pi}{B^2}\left[\frac{1}{JB_p}\frac{\partial}{\partial\psi}\left(p + \frac{B^2}{8\pi}\right)\hat{\boldsymbol{\psi}} - \frac{1}{JB_p}\frac{\partial}{\partial\chi}\left(\frac{B^2}{8\pi}\right)\frac{B_t}{B}\hat{\mathbf{t}}\right]. \tag{26}$$

In the above expression, it is convenient to remove all dependence on the plasma pressure. To do this, the Grad-Shafranov equation is used but with the toroidal current set to zero in agreement with our earlier assumptions. If this is done, the components of the curvature vector are found to be

$$\kappa_t = \boldsymbol{\kappa}\cdot\hat{\mathbf{t}} = -\frac{1}{2}\frac{B_t}{JB_pB^3}\frac{\partial B^2}{\partial\chi}, \tag{27}$$

$$\kappa_n = -\frac{RB_p}{2}\left[\frac{B_t^2}{B^2}\frac{\partial\log R^2}{\partial\psi} + \frac{B_p^2}{B^2}\frac{\partial\log J}{\partial\psi}\right]. \tag{28}$$

Substituting all of these expressions into the potential energy and kinetic energy, Eqs. (23) and (24) become

$$\begin{aligned} W(\psi) = \int Jd\chi \Bigg\{ & \frac{1}{J^2R^2B_p^2}\left[1 + \left(\frac{R^2B_p^2}{B}\int_{\chi_0}^{\chi}\frac{\partial\nu}{\partial\psi}d\chi'\right)^2\right]\left|\frac{\partial X}{\partial\chi}\right|^2 \\ & + 4\pi\frac{dp}{d\psi}\left[\frac{B_t^2}{B^2}\frac{\partial\log R^2}{\partial\psi} + \frac{B_p^2}{B^2}\frac{\partial\log J}{\partial\psi} + \frac{RB_t}{JB^2}\left(\int_{\chi_0}^{\chi}\frac{\partial\nu}{\partial\psi}d\chi'\right)\frac{\partial\log B^2}{\partial\chi}\right]|X|^2\Bigg\}, \end{aligned} \tag{29}$$

$$K = \pi\int d\psi d\chi\,\frac{J\rho}{R^2B_p^2}\left[1 + \left(\frac{R^2B_p^2}{B}\int_{\chi_0}^{\chi}\frac{\partial\nu}{\partial\psi}d\chi'\right)^2\right]|X|^2, \tag{30}$$

Further, from the energy principle, an Euler equation can be derived. The result is

$$\begin{aligned} 0 = & \frac{1}{J}\frac{\partial}{\partial\chi}\left\{\frac{1}{JB_p^2R^2}\left[1 + \left(\frac{R^2B_p^2}{B}\int_{\chi_0}^{\chi}\frac{\partial\nu}{\partial\psi}d\chi'\right)^2\right]\frac{\partial X}{\partial\chi}\right\} \\ & + \left\{\omega^2\frac{4\pi\rho}{R^2B_p^2}\left[1 + \left(\frac{R^2B_p^2}{B}\int_{\chi_0}^{\chi}\frac{\partial\nu}{\partial\psi}d\chi'\right)^2\right]\right. \\ & \left. - 4\pi\frac{dp}{d\psi}\left[\frac{B_t^2}{B^2}\frac{\partial\log R^2}{\partial\psi} + \frac{B_p^2}{B^2}\frac{\partial\log J}{\partial\psi} + \frac{RB_t}{JB^2}\left(\int_{\chi_0}^{\chi}\frac{\partial\nu}{\partial\psi}d\chi'\right)\frac{\partial\log B^2}{\partial\chi}\right]\right\}X. \end{aligned} \tag{31}$$

At this point, substantial simplifications can be made if the orderings of the physical problem are observed. First, we expand R in the vicinity of the null. If R_0 is the major radius of the null-point, then from Fig. 1, it is clear that

$$R = R_0 + x' = R_0 + \cos(\alpha)x + \sin(\alpha)z. \tag{32}$$

Further, because we assume that $R_0 \gg |x|, |z|$,

$$\frac{\partial \log R^2}{\partial \psi} \ll \frac{\partial \log J}{\partial \psi}. \tag{33}$$

At the same time, the toroidal field in the vicinity of the null is much larger than the poloidal field, $B_t \gg B_p$. Using these relations, consider the expression, $\partial\nu/\partial\psi$. Because we expect $\beta_t = 8\pi p/B_t^2 \ll 1$ in the divertor region, i.e. the toroidal magnetic pressure is much greater than the plasma pressure, the toroidal field is well-approximated by its vacuum solution. This implies that the quantity $B_t R$ is constant. Combining all of this,

$$\frac{\partial \nu}{\partial \psi} = B_t R \frac{\partial}{\partial \psi}\left(\frac{J}{R^2}\right) \approx \frac{B_0}{R_0}\frac{\partial J}{\partial \psi}, \tag{34}$$

where the toroidal field and major radius have been approximated by their values at the null-point, B_0 and R_0, respectively. Further, using Eq. (14) and $B \approx B_t \approx B_0$,

$$\frac{R^2 B_p^2}{B}\int_{\chi_0}^{\chi} \frac{\partial \nu}{\partial \psi} d\chi' \approx \frac{1}{J}\int_{\chi_0}^{\chi} \frac{\partial J}{\partial \psi} d\chi' \equiv s. \tag{35}$$

In this context, s corresponds to the shear in the magnetic field integrated along the poloidal coordinate, as will be shown later in this section. Next, if we consider the quantity, $\partial B^2/\partial\chi$, the same approximations can be used to show that

$$\frac{\partial \log B^2}{\partial \chi} \approx -\frac{\partial \log R^2}{\partial \chi} - \frac{B_p^2}{B_0^2}\frac{\partial \log J}{\partial \chi}. \tag{36}$$

Using these results and the orderings mentioned above, Eq. (31) simplifies to

$$\begin{aligned} 0 = \frac{1}{RJ}\frac{\partial}{\partial \chi}\left[\left(1+s^2\right)\frac{\partial X}{\partial \chi}\right] + \Bigg\{ \omega^2 \frac{4\pi\rho}{R^2 B_p^2}\left(1+s^2\right) \\ -4\pi \frac{dp}{d\psi}\left[\left(\frac{\partial \log R^2}{\partial \psi} + \frac{B_p^2}{B_0^2}\frac{\partial \log J}{\partial \psi}\right) - \left(\frac{\partial \log R^2}{\partial \chi} + \frac{B_p^2}{B_0^2}\frac{\partial \log J}{\partial \chi}\right) s\right]\Bigg\} X. \end{aligned} \tag{37}$$

At this point, it is simply a matter of applying Eq. (37) to the relevant divertor configurations. Before doing this, it is important to understand the meaning of the physical constant, χ_0, present in the definition of s. Hameiri made the observation that χ_0 corresponds to the polarization of the electric field[22]. This is easily seen from Ohm's law in the form

$$\mathbf{E} = \frac{i\omega}{c}\boldsymbol{\xi} \times \mathbf{B} = \frac{i\omega}{c} X \frac{\mathbf{k}_\perp}{n}, \tag{38}$$

$$= \frac{i\omega}{c} X \frac{B}{RB_p}\left[\hat{\mathbf{t}} - \frac{1}{J}\int_{\chi_0}^{\chi} \frac{\partial J}{\partial \psi} d\chi' \hat{\boldsymbol{\psi}}\right]. \tag{39}$$

From the above expression and Eq. (20), it is clear that χ_0 corresponds to the point at which the electric field is oriented completely in the geodesic direction and all plasma displacement is normal to the flux surface. Further, at points along the field line away from χ_0, the normal component of the electric field grows relative to the geodesic component and a geodesic component of the plasma displacement begins to shear the perturbations. Thus, an initial perturbation is distorted in the geodesic direction as it moves along the field line away from the point, χ_0. In the absence of shear, the electric field would lie solely in the geodesic direction and all plasma displacements would be normal to the flux surface.

We now apply the differential equation to the specific geometries found in the standard and snowflake divertors. To do so, we first consider the derivatives, $\partial \log R^2/\partial\psi$ and $\partial \log R^2/\partial\chi$. These derivatives can be computed as follows. First, from Eq. (9), we solve for $x+iz$ in terms of η, resulting in

$$x + iz = am^{1/m}\left(\frac{\eta}{CB_{pM}Ra}\right)^{1/m}. \tag{40}$$

From the above equation, the desired derivatives can be computed by differentiating Eq. (32) consistent with the large R_0 approximation. When this is done, the following equations result,

$$\frac{\partial \log R^2}{\partial\psi} = \frac{2}{R_0}\mathrm{Re}\left[\frac{d(x+iz)}{d\eta}e^{-i\alpha}\right], \tag{41}$$

$$\frac{\partial \log R^2}{\partial\chi} = -\frac{2}{R_0}\mathrm{Im}\left[\frac{d(x+iz)}{d\eta}e^{-i\alpha}\right], \tag{42}$$

The derivatives are easily computed from this form, and result in

$$\frac{\partial \log R^2}{\partial\psi} = \frac{2}{CR_0^2B_{pM}}\left(\frac{m^2(\psi^2+\chi^2)}{C^2R_0^2a^2B_{pM}^2}\right)^{\frac{1-m}{2m}}\cos(\alpha+\delta), \tag{43}$$

$$\frac{\partial \log R^2}{\partial\chi} = \frac{2}{CR_0^2B_{pM}}\left(\frac{m^2(\psi^2+\chi^2)}{C^2R_0^2a^2B_{pM}^2}\right)^{\frac{1-m}{2m}}\sin(\alpha+\delta), \tag{44}$$

Here, δ represents physically the angle a vector normal to a flux surface forms with the x-axis. This angle is expressed as

$$\delta = \frac{m-1}{m}\tan^{-1}\left(\frac{\chi}{\psi}\right) + 2\pi j/m. \tag{45}$$

The parameter, j, represents a branch cut, and can take values, $j = 0, 1, 2, ..., m-1$, corresponding to the disjoint regions in Fig. 1. Since the specific orientation of the flux surfaces

is captured by the parameter α, we can set $j = 0$ without loss of generality. This causes us to restrict our attention to the flux surfaces bounded by the separatrix and enclosing the positive x-axis in Fig. 1, but allowing us to vary its precise orientation with respect to the major radius through the angle, α. For the above expressions, we simply choose $m = 2$ for the standard divertor and $m = 3$ for the snowflake as mentioned in Section II.

Next, we compute the derivatives, $\partial \log J/\partial\psi$ and $\partial \log J/\partial\chi$. This is easily done for general m by using Eq. (11), and results in the expressions

$$\frac{\partial \log J}{\partial \psi} = -\left(\frac{m-1}{m}\right)\frac{2\psi}{\psi^2+\chi^2}, \tag{46}$$

$$\frac{\partial \log J}{\partial \chi} = -\left(\frac{m-1}{m}\right)\frac{2\chi}{\psi^2+\chi^2}. \tag{47}$$

Further, using the relation for the jacobian, the shear, s, can be computed. This gives the integral relation,

$$s = -2\left(\frac{m-1}{m}\right)\left(1+\frac{\chi^2}{\psi^2}\right)^{\frac{m-1}{m}}\int_{\chi_0/\psi}^{\chi/\psi}\frac{dx}{(1+x^2)^{\frac{2m-1}{m}}}. \tag{48}$$

This integral can be evaluated for general m through the use of hypergeometric functions. For the standard divertor, the integral can be performed exactly and becomes

$$s = -\frac{\chi}{\psi} + \frac{\chi_0}{\psi}\sqrt{\frac{1+(\chi/\psi)^2}{1+(\chi_0/\psi)^2}}, \tag{49}$$

whereas in the case of the snowflake divertor, no expression in terms of elementary functions exists. Thus, in evaluating s for the snowflake, the integral can be performed numerically for arbitrary χ_0. For $\chi_0 = 0$, the two asymptotic forms can be used to compose an approximate form for s for the snowflake that agrees well over the range of x. These asymptotic forms are

$$s \sim -2\left(\frac{m-1}{m}\right)\frac{\chi}{\psi}, \qquad \frac{\chi}{\psi} \ll 1, \tag{50}$$

$$s \sim -2\left(\frac{m-1}{m}\right)\left[\int_0^\infty \frac{dx}{(1+x^2)^{\frac{2m-1}{m}}}\right]\left(\frac{\chi}{\psi}\right)^{\frac{2(m-1)}{m}}, \qquad \frac{\chi}{\psi} \gg 1, \tag{51}$$

Thus, for the snowflake, the function, s can be well approximated by

$$s \approx -\frac{4}{3}\frac{\chi}{\psi}\left(1+0.7554\left|\frac{\chi}{\psi}\right|\right)^{1/3}, \tag{52}$$

with the constant, 0.7554, found by numerically performing the integral in Eq. (51).

Finally, Eq. (14) allows an expression for B_p^2 to be quickly found as expressions for the jacobian have already been given, and R can simply be approximated as R_0, consistent with our approximations. With these expressions, the differential equation modeling ballooning modes can be written specifically for the two divertor configurations we are considering. To do so, it is useful to scale the equations so that the dimensionless parameters are clearly apparent. This is done through the relations

$$\psi \to CR_0 a B_{pM} \psi, \tag{53}$$

$$\chi \to CR_0 a B_{pM} \chi. \tag{54}$$

Further, it is convenient to replace the variable χ with $x = \chi/\psi$ as this is the natural scaling for the poloidal coordinate. This greatly simplifies the resulting equations. The differential equation for the standard divertor becomes

$$\begin{aligned} -\frac{\partial}{\partial x}\left[(1+s^2)\frac{\partial X}{\partial x}\right] + \beta_{pM}\frac{d\log p}{d\log\psi}\left[\frac{a}{2\sqrt{2}C^2R_0\psi^{1/2}}\frac{\cos(\alpha+\delta)-s\sin(\alpha+\delta)}{(1+x^2)^{3/4}}\right. \\ \left. -\frac{B_{pM}^2}{2B_0^2}\frac{1-sx}{1+x^2}\right]X = \frac{\omega^2 a^2}{4C^2 v_{AM}^2}\frac{1+s^2}{1+x^2}X. \end{aligned} \tag{55}$$

In the above equation, $\beta_{pM} = 8\pi p/B_{pM}^2$ and $v_{AM}^2 = B_{pM}^2/4\pi\rho$. Performing the same steps for the snowflake divertor, the result is

$$\begin{aligned} -\frac{\partial}{\partial x}\left[(1+s^2)\frac{\partial X}{\partial x}\right] + \beta_{pM}\frac{d\log p}{d\log\psi}\left[\frac{a}{18C^2R_0\psi}\frac{\cos(\alpha+\delta)-s\sin(\alpha+\delta)}{1+x^2}\right. \\ \left. -\frac{B_{pM}^2}{3B_0^2}\frac{1-sx}{1+x^2}\right]X = \frac{\omega^2 a^2}{3^{8/3}C^2 v_{AM}^2\psi^{2/3}}\frac{1+s^2}{(1+x^2)^{4/3}}X. \end{aligned} \tag{56}$$

To evaluate the derivative $d\log p/d\log\psi$, we assume that the full pressure drops over the width between the flux surfaces, $\psi = 0$ and $\psi = \Delta_M/a$. The latter flux surface corresponds to the flux surface at the edge of the SOL. Thus, the derivative becomes

$$\frac{d\log p}{d\log\psi} \approx \frac{\Delta p/p}{\Delta\psi/\psi} \approx -1. \tag{57}$$

Finally, in both Eqs. (55) and (56), we use Dirichlet boundary conditions for X to reflect the line-tying boundary conditions. If the distance from the null to the plates along the separatrix is L, this translates to a value of $x = \pm L^2/2\Delta_M a$ for the standard divertor and $x = \pm L^3/3\Delta_M a^2$ for the snowflake divertor. Typically, these values of x are much greater than unity, and in the next section we will neglect the plates all together. This is valid so

long as the eigenfunctions are localized to small values of x, which will be the case due to the increasing shear with increasing x.

We close this section with a discussion on shear. Analysis of shear in the snowflake divertor has been performed elsewhere[24]. In what follows, a slightly different presentation is given in order to elucidate the relevance of the shear to the problem considered here. The relative strength of the shear in the snowflake as compared to the standard divertor is somewhat misleading from the form of Eqs. (49) and (52). The fact that s grows faster in the snowflake than in the standard divertor as a function of χ/ψ reflects the fact that for a given poloidal distance traversed, s will be larger in the snowflake case. However, because of the smaller poloidal field in the snowflake, this corresponds to many more toroidal transits and a much larger distance along the field line will have been traversed. To see this more clearly, we first find the position of a field line poloidally as it moves toroidally around the device. We set $C = 1$ in what follows as its precise value is unimportant for this discussion. We start at the point $x = x_0$, $z = 0$. Since the field lines are confined to surfaces of constant ψ, this gives us a relation between x and z along the ray's trajectory. For the standard divertor, the trajectory of the rays is governed by

$$\frac{dx}{z} = \frac{dz}{x} = \frac{d\zeta}{q^*}, \tag{58}$$

where $q^* = aB_0/RB_{pM}$. Further, constant ψ requires that $x_0^2 = x^2 - z^2$. Integrating the above equation gives

$$x = x_0 \cosh\left(\frac{\zeta - \zeta_0}{q^*}\right), \tag{59}$$

$$z = x_0 \sinh\left(\frac{\zeta - \zeta_0}{q^*}\right). \tag{60}$$

Substituting these results into Eq. (49) with $\chi_0 = 0$ results in

$$s = -\sinh\left(\frac{2\,(\zeta - \zeta_0)}{q^*}\right) \approx -\frac{2\,(\zeta - \zeta_0)}{q^*}, \tag{61}$$

where the approximate form is for small argument. Doing the same procedure for the snowflake,

$$\frac{dx}{2xz} = \frac{dz}{x^2 - z^2} = \frac{d\zeta}{aq^*}. \tag{62}$$

Constant ψ requires that $x_0^3 = x^3 - 3xz^2$. Solving for z and substituting into the above equation results in

$$\int_{x_0}^{x} \frac{1}{2}\sqrt{\frac{3}{x'(x'^3 - x_0^3)}}dx' = \frac{\zeta - \zeta_0}{aq^*}. \tag{63}$$

This integral can be approximated for values of x close to x_0. If this is done, expressions for x and z are,

$$x = x_0 + x_0^3 \left(\frac{\zeta - \zeta_0}{a q^*} \right)^2, \tag{64}$$

$$z = x_0^2 \left(\frac{\zeta - \zeta_0}{a q^*} \right). \tag{65}$$

Plugging this into the asymptotic expression for s for $\chi/\psi \ll 1$, results in

$$s = -4 \frac{x_0}{a} \frac{\zeta - \zeta_0}{q^*}. \tag{66}$$

From here, it is apparent that the shear is smaller for a given toroidal distance travelled in the snowflake by a factor of x_0/a. For a given SOL width in the midplane, Δ_M, the distance closest to the null is $x_0/a = (3\Delta_M/a)^{1/3}$. This is typically a small factor, though the greater fanning of the flux surfaces near the null results in the exponent 1/3, which can make the shear comparable for the two divertor configurations.

IV. INSTABILITY THRESHOLD

The next step is to be able to determine the thresholds for instability for Eqs. (55) and (56). This amounts to determining the value of β_{pM} for which $\omega^2 = 0$. Further, for a given value of β_{pM}, the parameter, $\Gamma = \omega^2 a^2 / v_{AM}^2$ can be determined. To do so, we employ a variational approach in which we use a test function to approximate the fundamental mode of the differential equation. For this reason, the thresholds reported are sufficient conditions for instability, but they are not necessary. Further, we set $\chi_0 = 0$. This is done because we are interested in modes which are unstable in the vicinity of the null point where the poloidal field is small. A more detailed numerical analysis could be performed in which different values of χ_0 are explored, but we leave this for applications to specific experimental devices as the methodology developed below will be directly applicable in those cases. It should be mentioned that in choosing values of χ_0, it is important that the spatial positions still satisfy the length scales of the problem, i.e. that $r/a \ll 1$.

We first consider the standard divertor. In this case, the choice of $\chi_0 = 0$ greatly simplifies the differential equation into the form

$$-\frac{\partial}{\partial x}\left[(1+x^2)\frac{\partial X}{\partial x}\right] - \beta_{pM}\left[\frac{a}{2\sqrt{2}C^2 R_0 \psi^{1/2}} \frac{\cos(\alpha+\delta) + x\sin(\alpha+\delta)}{(1+x^2)^{3/4}} - \frac{B_{pM}^2}{2B_0^2}\right] X = \frac{\omega^2 a^2}{4C^2 v_{AM}^2} X. \tag{67}$$

Casting the equation into a variational form is easily done by multiplying by X and then integrating over the domain. The trial function chosen is of the form

$$X = \sqrt{\frac{1}{\pi\,(1+x^2)}}. \tag{68}$$

This choice enables most of the integrals to be performed analytically. Further, because $|X|^2$ converges to zero as $1/x^2$, the conducting planes can be approximately neglected as these conditions are enforced at large values of x as mentioned in Section III. Performing the resulting integrals,

$$\int_{-\infty}^{\infty} \left(1+x^2\right) \left|\frac{\partial X}{\partial x}\right|^2 \, dx = \frac{1}{2}, \tag{69}$$

$$\int_{-\infty}^{\infty} \frac{\cos(\alpha+\delta) + x\sin(\alpha+\delta)}{(1+x^2)^{3/4}} \, |X|^2 \, dx \approx \frac{1}{\sqrt{2}} \cos\alpha, \tag{70}$$

$$\int_{-\infty}^{\infty} |X|^2 \, dx = 1. \tag{71}$$

In evaluating Eq. (70), the odd portion of the integrand vanishes. For nonzero values of χ_0, this would not be the case, and an additional term proportional to $\sin\alpha$ would appear. This would have the effect of shifting the argument of the cosine on the right hand side of Eq. (70) by some angle, and it would change the the numerical coefficient. Both of these effects would display a complicated dependency on the value of χ_0. In our case, the resulting integral is performed numerically due to the factors of $\cos\delta$ and $\sin\delta$ that appear. The resulting numeric integral is close to the factor $1/\sqrt{2}$, and we make this approximation for simplicity of expression. Upon performing the integrals, the following equation results,

$$1 - \beta_{pM}\left(\frac{a}{2C^2R_0}\left(\frac{a}{\Delta_M}\right)^{1/2}\cos\alpha - \frac{B_{pM}^2}{B_0^2}\right) = \frac{\omega^2}{2C^2a^2v_{AM}^2}, \tag{72}$$

where in the above expression, the choice $\psi = \Delta_M/a$ has been used, consistent with earlier approximations. The above equation can be written in a simple form if the factor of B_{pM}^2/B_0^2 is factored out and the definition

$$\cos\alpha_c = 2C^2\frac{R_0}{a}\frac{B_{pM}^2}{B_0^2}\left(\frac{\Delta_M}{a}\right)^{1/2} = \frac{2C^2}{q^{*2}}\frac{(\Delta_M a)^{1/2}}{R}, \tag{73}$$

is made, with $q^* = aB_0/RB_{pM}$. Further, we define $\Gamma = \omega^2a^2/v_{AM}^2$. With these designations, the equation becomes

$$\Gamma = -2C^2\left[\beta_t\left(\frac{\cos\alpha}{\cos\alpha_c} - 1\right) - 1\right], \tag{74}$$

and the instability threshold becomes

$$\beta_{pM} > \frac{2C^2 \frac{R}{a} \left(\frac{\Delta_M}{a}\right)^{1/2}}{\cos\alpha - \cos\alpha_c}. \tag{75}$$

The presence of a critical angle introduces an additional constraint that must also be satisfied, namely that $\cos\alpha_c < 1$, in order for the above threshold to be valid.

Using the same procedure, we next examine ballooning instability in a snowflake divertor. In this case, it is more appropriate to use a more rapidly converging test function. This is the case because of the decreased shear present in the snowflake. For this reason, we confine ourselves somewhat poloidally, realizing that many toroidal transits are occurring over this shorter poloidal distance. It is also important that the test function not converge too rapidly as this would maximize the energy created by line-bending in the differential equation, resulting in robust stability. For these reasons, we choose the test function,

$$X = \sqrt{\frac{3}{8\pi}} \frac{1}{1+x^2}. \tag{76}$$

Higher powers of $1/(1+x^2)^n$ have also been considered, but this choice gave the lowest instability threshold. For the shear, the approximation given by Eq. (52) is used. Because of the complicated form of s, all integrals are performed numerically. Using the same procedure as in the standard divertor case results in the equations

$$\Gamma = -\left(\frac{\Delta_M}{a}\right)^{2/3} C^2 \left[\frac{I_3}{I_4}\beta_t \frac{a}{\Delta_M}\left(\frac{\cos\alpha}{\cos\alpha_c} - 1\right) - \frac{I_1}{I_4}\right], \tag{77}$$

$$\cos\alpha_c = \frac{I_3}{I_2}\frac{aC^2}{Rq^{*2}}, \tag{78}$$

$$\beta_{pM} > C^2 \frac{I_1}{I_2} \frac{\frac{R\Delta_M}{a^2}}{\cos\alpha - \cos\alpha_c}. \tag{79}$$

In the above expressions, the values of I_j are given by

$$I_1 = \int_{-\infty}^{\infty} (1+s^2) \left|\frac{\partial X}{\partial x}\right|^2 dx, \tag{80}$$

$$I_2 = \frac{1}{18}\int_{-\infty}^{\infty} \frac{\cos\delta - s\sin\delta}{1+x^2} |X|^2 \, dx, \tag{81}$$

$$I_3 = \frac{1}{3}\int_{-\infty}^{\infty} \frac{1-xs}{1+x^2} |X|^2 \, dx, \tag{82}$$

$$I_4 = \frac{1}{3^{8/3}}\int_{-\infty}^{\infty} \frac{1+s^2}{(1+x^2)^{4/3}} |X|^2 \, dx. \tag{83}$$

For the specific test function we have chosen, the expressions become

$$\Gamma = -\left(\frac{\Delta_M}{a}\right)^{2/3} C^2 \left[6.04\,\beta_t \frac{a}{\Delta_M}\left(\frac{\cos\alpha}{\cos\alpha_c} - 1\right) - 31.5\right], \tag{84}$$

$$\cos\alpha_c = 8.3\,C^2 \frac{a}{Rq^{*2}}, \tag{85}$$

$$\beta_{pM} > 43.2\,C^2 \frac{\frac{R\Delta_M}{a^2}}{\cos\alpha - \cos\alpha_c}. \tag{86}$$

If the distance of closest approach of the flux surface to the null point, d, is related to the width of the SOL in the midplane, the equation, $d^3 = 3\Delta_M a^2$ results. Rewriting the instability threshold for β_t, we see that it scales as

$$\beta_t > 14.4\,C^2 \frac{\frac{d^3}{Ra^2q^{*2}}}{\cos\alpha - \cos\alpha_c}. \tag{87}$$

If $\alpha = 0$ and the critical angle is set to $\pi/2$, this result agrees with the simple scalings first reported by Ryutov et al.[15]. The critical angle, which can be traced to terms proportional to derivatives of the jacobian, is an effect due to the convergence of the field lines away from the null point and could not be captured by the simple arguments previously reported.

V. CONCLUSIONS

Using Ideal MHD theory, instability thresholds are reported which clearly show the scalings and the dependence on the relevant parameters in both the standard and snowflake divertor configurations. The presence of a critical angle introduces an additional requirement for instability. This has been shown to be caused by the variation of the jacobian with spatial position and is a geometrical effect due to the field-line topologies encountered in the presence of a poloidal field null. It occurs in addition to the requirement that unfavorable curvature be present along the flux surface. The possibility of ballooning modes in a standard divertor could be important if it leads to heat flux broadening. At a more fundamental level, this theory places a limit on the steepness of the pressure gradient and would place a floor on the characteristic width of the plasma in the private flux region. This feature is also present in the snowflake divertor, with the addition that new strike points can now be activated through turbulent mixing caused by the nonlinear evolution of the ballooning mode.

We apply the resulting limits to the cases of NSTX, DIII-D, TCV, and an ITER-like device in Table I. Characteristic values for q^*, a/R, and Δ_M/R are given, and C is set to

TABLE I. Instability threshold applied to various tokamaks

				Standard divertor		Snowflake divertor	
Tokamak	q^*	a/R	Δ_M/R	α_c	$\beta_{pM,c}$	α_c	$\beta_{pM,c}$
NSTX[7,25,26]	1.60	0.80	7.1×10^{-3}	86.6°	0.24	$\cos\alpha_c > 1$	N/A
DIII-D[26]	3.17	0.40	2.1×10^{-3}	89.7°	0.36	70.7°	0.56
TCV[14,25,27]	2.03	0.28	9.1×10^{-3}	88.6°	1.3	55.7°	5.0
ITER[28]	3	0.32	1.6×10^{-4}	89.9°	0.14	72.8°	6.8×10^{-2}

unity. From these values, the instability thresholds are computed for both the standard and snowflake divertor configurations. The instability thresholds are given in the form

$$\beta_{pM} > \frac{\beta_{pM,c}}{\cos\alpha - \cos\alpha_c}, \tag{88}$$

with α_c and $\beta_{pM,c}$ given in the table. For NSTX in the snowflake case, the modes are robustly stable. Even in the standard case, the threshold given is large enough that instability would not occur except during a large ELM event. For TCV, the situation is somewhat improved, in that instability is at least possible in the snowflake case. However, the resulting threshold is too large to be realistic. From this table, we conclude that this mode is unlikely to explain the results observed in NSTX and TCV. Considering DIII-D parameters offer a slight improvement, due to a smaller SOL width, but the limits given are still too high to be of relevance. Examining conditions relevant to ITER, we see the lowest thresholds for the standard divertor and snowflake. This is largely due to the much lower value of Δ_M/R. The smaller SOL width is projected by a theory developed by Goldston and Eich[28] which scales well with existing devices. This instability could expand the heat flux and lead to convective mixing during an ELM when a snowflake divertor is used if the projected SOL width is correct. For ITER, a generic value of q^* is chosen in order to make estimates.

This theory can also be applied in the private flux region in order to ascertain whether these modes could be responsible for the observed heat flux width in this region. In doing so, we set $\cos\alpha = 1$ and assume $\cos\alpha_c \ll 1$. The resulting values of Δ_M justify the latter assumption. Further, the quantity, Δ_M/a is now replaced with the dimensionless flux function, ψ. The resulting flux function can then be expressed in terms of the distance from the null point, d, which is unstable, $\psi = d^2/2a^2$ for the standard divertor and $\psi = d^3/3a^3$ for the snowflake. The pressure drive is assumed to be provided by plasma transported from the

TABLE II. Lower bound for width of flux in private flux region during Inter-ELM operation

			Standard divertor		Snowflake divertor	
Tokamak	a/R	β_{pM} (Inter-ELM)	μ	d (cm)	μ	d (cm)
NSTX	0.80	$> 6 \times 10^{-3}$	5×10^{-4}	0.2	1×10^{-2}	5
DIII-D	0.40	$> 3.5 \times 10^{-3}$	1×10^{-4}	7×10^{-2}	1×10^{-2}	3
TCV	0.28	$\sim 6 \times 10^{-3}$	2×10^{-5}	3×10^{-2}	1×10^{-3}	1

SOL towards the divertor region, so characteristic values for β_{pM} are used. The instability thresholds then become

$$\psi_c = \frac{d^2}{2a^2} < \frac{1}{4}\frac{a^2}{R^2}\beta_{pM}^2, \tag{89}$$

for the standard divertor and

$$\psi_c = \frac{d^3}{3a^3} < \frac{1}{43.2}\frac{a}{R}\beta_{pM}, \tag{90}$$

for the snowflake. A ratio can then be defined of the unstable flux to the flux that characterizes the SOL, i.e. $\mu = \psi_c/(\Delta_M/a)$. This parameter is given so that as the field lines converge away from the null point, a meaningful width near the divertor plates can be determined. Again, attempting to pick parameters relevant to existing devices, we give both the ratio, μ, and the distance from the null point, d, that would be unstable in the private flux region in Table II. The results give values that are likely too small to be of interest to the SOL for Inter-ELM operation. During an ELM, however, the value of β_{pM} can increase by a factor of $10 - 30$. In this case, the values of μ will increase in the table by a factor of $100 - 900$ for the standard divertor and $10 - 30$ for the snowflake. These results would give a floor to the observed widths of the heat flux in the private flux region during an ELM event. The theory would need to compared in more detail with experimental data for a given device to determine if this mechanism is indeed responsible. It would be necessary to account for the contraction of the flux as it moves from the null point towards the divertor plates.

To explain the enhanced transport observed in TCV, new importance is given to a toroidally axisymmetric mode[16] which is more likely to explain the heat fluxes observed in the private flux regions on TCV[13,14]. While this toroidally axisymmetric mode was considered in a model geometry[16], it would be important to perform similar analysis that retains the complex geometrical effects present. The additional complication is that the resulting

problem is inherently two-dimensional, and is not amenable to the one-dimensional reduction that occurs in the ballooning limit. The third possibility that the equilibrium is lost altogether[15] should also be investigated.

ACKNOWLEDGMENTS

The author is grateful to Dr. D. D. Ryutov for many helpful discussions regarding the material and for suggestions that have improved the content of this manuscript. This work was performed under the auspices of the U.S. Department of Energy by Lawrence Livermore National Laboratory under Contract DE-AC52-07NA27344.

APPENDIX

Here, we consider the case of a straight poloidal field with no null, i.e. the $m = 1$ case in Section II. Instead of the designation that $|\nabla\psi| = |\nabla\chi|$, we choose that $\psi = \int_0^x RB_p\, dx'$ and $\chi = z$. The jacobian is easily computed and is $J = 1/B_p$. In order that we have a valid equilibrium, R must be aligned with the x-axis and $\alpha = 0$. Computing first the gradient of the eikonal, it can be shown that

$$k_t = n\frac{1}{R}\frac{B}{B_p}, \tag{91}$$

$$k_n = -n\frac{\partial}{\partial x}\left[\frac{B_t}{RB_p}\right](z - z_0). \tag{92}$$

Further, the curvature is solely in the normal direction with no geodesic curvature present. Thus,

$$\boldsymbol{\kappa} = -\frac{B_t^2}{RB^2}\hat{\mathbf{x}}. \tag{93}$$

Substituting these expressions into Eq. (23) gives

$$W(\psi) = \int \frac{dz}{R^2 B_p}\left[\left(1 + \left(\frac{B_t}{B}\frac{\nu'}{\nu}(z - z_0)\right)^2\right)\left|\frac{\partial X}{\partial z}\right|^2 + \frac{8\pi p}{B^2}\frac{B_t^2}{B_p^2}\frac{p'}{pR}|X|^2\right], \tag{94}$$

where, in this case, $\nu = B_t/RB_p$ and a prime denotes a derivative with respect to R which

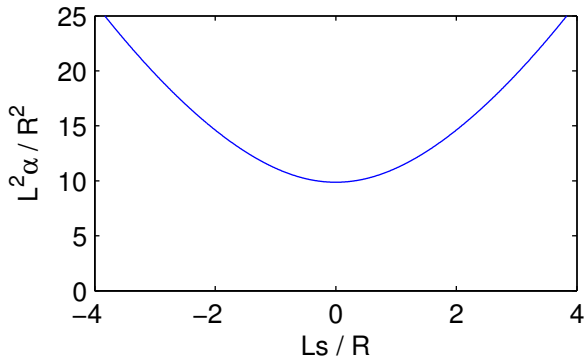

FIG. 2. Instability threshold for ballooning modes with a vertical poloidal field and azimuthal toroidal field. Horizontal axis is the product of the shear, s, given by Eq. (95) with the distance between conducting planes, L, divided by the major radius, R. The vertical axis gives the instability threshold for the parameter, α, given by Eq. (96) multiplied by L^2/R^2. Instability exists when parameters fall above the curve.

is equivalent to a derivative with respect to x. If we define the following parameters,

$$s = \frac{B_t}{B}\frac{d\log\nu}{d\log R}, \tag{95}$$

$$\alpha = \beta_p \frac{B_t^2}{B^2}\left|\frac{d\log p}{d\log R}\right|, \tag{96}$$

and scale the z, coordinate to the distance between the plates, L, by making the transformation, $z' = z/L$, the potential energy can be rewritten as

$$W(\psi) = \int \frac{dz}{R^2L^2B_p}\left[\left(1+\left(\frac{sL}{R}(z'-z_0')\right)^2\right)\left|\frac{\partial X}{\partial z'}\right|^2 - \frac{L^2}{R^2}\alpha\left|X\right|^2\right]. \tag{97}$$

From the above expression, a differential equation can be found which governs the eigenfunctions that exist at marginal stability. This is given by

$$\frac{\partial}{\partial z'}\left[\left(1+\left(\frac{sL(z'-z_0')}{R}\right)^2\right)\frac{\partial X}{\partial z'}\right] + \frac{L^2}{R^2}\alpha X = 0, \tag{98}$$

with X on the domain, $z' \in (-1/2, 1/2)$. From the potential energy formulation, it is clear that we want to minimize the shear term, so $z_0' = 0$ should result in the minimum instability threshold. If the shear is negligible, the most unstable mode is given by

$$X = C\cos\left(\pi z'\right), \tag{99}$$

and results in the instability threshold that

$$\alpha > \frac{\pi^2 R^2}{L^2}. \tag{100}$$

Further, it is a simple matter to numerically compute the instability threshold as a function of the shear as this can be easily done with existing routines. Figure 2 plots the instability threshold as a function of shear. If we assume that the poloidal field is constant with radius, that the poloidal field is small relative to the toroidal field so that $B_t \approx B$, and that the toroidal field is well approximated by its vacuum solution, i.e. that $\beta_t \ll 1$, then $s = -2$. Further, to compare the instability threshold to that in Ref. 16, we take $R/L = 5$. This gives the instability threshold of $\alpha > 252$. The derivative, $|d \log p / d \log R| = R/L_p$, where L_p is the characteristic length scale over which the pressure gradient drops. If we take this to be the width of the SOL, the instability threshold results in $\beta_p > 2.3$. This is much lower than the instability thresholds reported in Ref. 16. However, the ballooning modes are much more sensitive to the effects of shear, so it is possible that in a realistic divertor configuration, the axisymmetric mode would be of greater relevance.

REFERENCES

[1]D. D. Ryutov, Phys. Plasmas **14**, 064502 (2007).

[2]D. D. Ryutov, M. A. Makowski, and M. V. Umansky, Plasma Phys. Control. Fusion **52**, 105001 (2010).

[3]M. V. Umansky, T. D. Rognlien, D. D. Ryutov, and P. B. Snyder, Contrib. Plasma Phys. **50**, 350 (2010).

[4]D. D. Ryutov, R. H. Cohen, T. D. Rognlien, and M. V. Umansky, Contrib. Plasma Phys. **52**, 539 (2012).

[5]D. D. Ryutov, R. H. Cohen, T. D. Rognlien, and M. V. Umansky, Plasma Phys. Controlled Fusion **54**, 124050 (2012).

[6]D. D. Ryutov and M. V. Umansky, Phys. Plasmas **20**, 092509 (2013).

[7]V. A. Soukhanovskii, R. E. Bell, A. Diallo, S. Gerhardt, S. Kaye, E. Kolemen, B. P. Leblanc, A. G. McLean, J. E. Menard, S. F. Paul, M. Podesta, R. Raman, T. D. Rognlien, A. L. Roquemore, D. D. Ryutov, F. Scotti, M. V. Umansky, D. Battaglia, M. G. Bell, D. A. Gates, R. Kaita, R. Maingi, D. Mueller, and S. A. Sabbagh, Phys. Plasmas 19, 082504 (2012).

[8]V. A. Soukhanovskii, J.-W. Ahn, R. E. Bell, D. A. Gates, S. Gerhardt, R. Kaita, E. Kolemen, B. P. LeBlanc, R. Maingi, M. Makowski, R. Maqueda, A. G. McLean, J. E. Menard, D. Mueller, S. F. Paul, R. Raman, A. L. Roquemore, D. D. Ryutov, S. A. Sabbagh, and H. A. Scott, Nucl. Fusion 51, 012001 (2011).

[9]F. Piras, S. Coda, I. Furno, J.-M. Moret, R. A. Pitts, O. Sauter, B. Tal, G. Turri, A. Bencze, B. P. Duval, F. Felici, A. Pochelon, and C. Zucca, Plasma Phys. Controlled Fusion 51, 055009 (2009).

[10]F. Piras, S. Coda, B. P. Duval, B. Labit, J. Marki, S. Yu Medvedev, J.-M. Moret, A. Pitzschke, and O. Sauter, Plasma Phys. Controlled Fusion 52, 124010 (2010).

[11]F. Piras, S. Coda, B. P. Duval, B. Labit, J. Marki, S. Yu. Medvedev, J.-M. Moret, A. Pitzshke, and O. Sauter, Phys. Rev. Lett. 105, 155003 (2010).

[12]S. L. Allen, T. H. Osborne, E. Kolemen, J. Boedo, N. Brooks, M. Fenstermacher, R. Groebner, D. N. Hill, A. Hyatt, C. Lasnier, A. Leonard, M. Makowski, W. H. Meyer, A. McLean, T. Petrie, D. Ryutov, and J. Watkins, Initial snowflake divertor physics studies on DIII-D, Paper PD/1-2 at 24th IAEA FECIAEA CN-197, San Diego, 813 October 2012, available at https://fec2012.iaea.org/.

[13]W. A. J. Vijvers, J. P. Canal, B. Labit, H. Reimerdes, B. Tal, S. Coda, B. P. Duval, T. Morgan, G. de Temmerman, J. J. Zielinski, and the TCV team, Reduction of Peak Wall Power Loads in L- and H-mode Tokamak Plasmas in TCV with the Snowake Divertor, Paper EX/P5-22 at 2012 IAEA Fusion Energy Conference, San-Diego, October 812, 2012, available at https://fec2012.iaea.org/.

[14]H. Reimerdes, G. P. Canal, B. Labit, W. A. J. Vijvers, S. Coda, B. P. Duval, T. Lunt, T. Morgan, B. Tal, G. De Temmerman, and TCV Team, Plasma Phys. Contr. Fusion 55, 124027 (2013).

[15]D. D. Ryutov, R. H. Cohen, E. Kolemen, L. LoDestro, M. Makowski, J. Menard, T. D. Rognlien, V. A. Soukhanovskii, M. V. Umansky, and X. Xu, in *Proceedings of the 24th IAEA Fusion Energy Conference*, San Diego, USA, 2012, TH/P4-18.

[16]W. A. Farmer and D. D. Ryutov, Phys. Plasmas **20**, 092117 (2013).

[17]J. W. Connor, R. J. Hastie, and J. B. Taylor, Proc. R. Soc. Lond. A, **365**, 1 (1979).

[18]J. P. Freidberg, *Ideal Magnetohydrodynamics* (Plenum, New York, 1987).

[19]W. B. Kunkel and J. U. Guillory, *Proceedings of the 7th International Conference on Phenomena in Ionized Gases*, edited by B. Perovic and D. Tosic (Gradevinska Knjiga,

Belgrade, Yugoslavia, 1996), Vol. II, p. 702.

[20]J. R. Myra, D. A. D'Ippolito, and J. P. Goedbloed, Phys. Plasmas **4**, 1330 (1997).

[21]F. D. Halpern, S. Jolliet, J. Loizu, A. Mosetto, and P. Ricci, Phys. Plasmas **20**, 052306 (2013).

[22]E. Hameiri, Phys. Plasmas **6**, 674 (1998).

[23]A. J. Webster and C. G. Gimblett, Phys. Rev. Lett. **16**, 082502 (2009).

[24]D. D. Ryutov, R. H. Cohen, T. D. Rognlien, and M. V. Umansky, Phys. Plasmas, **15**, 092501 (2008).

[25]V. A. Soukhanovskii, R. E. Bell, A. Diallo, S. Gerhardt, S. Kaye, E. Kolemen, B. P. LeBlanc, A. McLean, J. E. Menard, S. F. Paul, M. Podesta, R. Raman, D. D. Ryutov, F. Scotti, R. Kaita, R. Maingi, D. M. Mueller, A. L. Roquemore, H. Reimerdes, G. P. Canal, B. Labit, W. Vijvers, S. Coda, B. P. Duval, T. Morgan, J. Zielinski, G. D. Temmerman, and B. Tal, J. Nucl. Mat. 438, S96 (2013).

[26]V. A. Soukhanovskii (private communication, 2014).

[27]W. A. J. Vijvers (private communication, 2014).

[28]R. J. Goldston and T. Eich, in *Proceedings of the 24th IAEA Fusion Energy Conference*, San Diego, USA, 2012, TH/P4-19.